ELSEVIER

Journal of Organometallic Chemistry 549 (1997) 295–304

Journal of Organometallic Chemistry

Synthesis and detailed NMR study of tricarbonylrhenium(I) and trimethylplatinum(IV) halide complexes of 2-methylthiomethyl-4-(S)-methyl-1,3-oxazoline (L). X-ray crystal structure of *fac*-[ReBr(CO)$_3$L]

Peter J. Heard [a,*], Derek A. Tocher [b]

[a] *Department of Chemistry, Birkbeck College, Gordon House, 29 Gordon Square, London WC1, UK*
[b] *Department of Chemistry, University College London, Christopher Ingold Laboratories, 20 Gordon Street, London WC1, UK*

Received 4 July 1997

Abstract

2-Methylthiomethyl-4-(S)-methyl-1,3-oxazoline (L) reacts with the halogenopentacarbonylrhenium(I) and halgenotrimethylplatinum(IV) metal moieties, to form complexes of general formulae *fac*-[ReX(CO)$_3$L] and *fac*-[PtXMe$_3$L] (X = Cl, Br or I) in good yield. Detailed NMR studies reveal the presence of four solution-state diasteroisomers, which differ according to the orientation of the S–Me and oxazole–methyl groups with respect to the halogen. Above ambient temperature, inversion at the S atom causes the epimerisation of pairs of diastereoisomers. The energetics of S inversion in the complexes [ReX(CO)$_3$L] (X = Cl, Br or I) were measured by standard ^{1}H band shape analysis of the variable temperature spectra; energy barriers, $\Delta G^{\ddagger}$ (298 K), are in the range 67–70 kJ mol^{-1}. Atropisomerisation occurs over a period of several hours at ca. 350 K, and several weeks at ca. 273 K. Platinum-195 NMR data are reported for the complexes [PtXMe$_3$L] (X = Cl, Br or I). © 1997 Elsevier Science S.A.

Keywords: Halogenopentacarbonylrhenium metal moiety; Halgenotrimethylplatinum(IV) metal moiety; NMR studies

1. Introduction

Enantiomerically pure oxazolines have been used as chiral auxiliary ligands in metal mediated asymmetric transformations for over twenty years [1,2]. The stereochemical control exerted by these auxiliaries is generally excellent, and consequently, they have found widespread use in both stoichiometric and, more recently, catalytic reactions [3]. Williams and coworkers [4] have prepared a variety of oxazolines with a secondary, hybrid donor (P or S), with the aim of modifying the chemical properties of the ligands, without affecting the stereo-control exerted by the oxazole. A number of catalytic systems incorporating these, and related acetal ligands have now been reported [5–11].

Our group embarked recently on a systematic study of the solution-state structures of, and fluxional rearrangements in 'chiral-at-ligand' organotransition metal complexes. The use of the C_2 symmetric bis(oxazoline), 2,6-bis[4-(S)-methyloxazolin-2-yl]pyridine, as a mechanistic probe for the fluxional rearrangements observed when potentially terdentate (meridinal) ligands have their bonding restricted to a bidentate mode, has been demonstrated [12]. We report here the results of a detailed NMR study on the solution-state structures of tricarbonylrhenium(I) halide complexes of 2-methylthiomethyl-4-(S)-methyl-1,3-oxazoline (L), namely *fac*-[ReX(CO)$_3$L] (X = Cl, Br or I). We also report on the analogous platinum(IV) complexes, *fac*-[PtXMe$_3$L] (X = Cl, Br or I).

2. Experimental details

2.1. Synthesis of complexes

All manipulations were carried out under an atmosphere of dry, oxygen-free nitrogen, using standard

* Corresponding author.

PII S0022-328X(97)00530-5

Schlenk techniques [13]. Solvents were dried [14] and degassed before use. The ligand, 2-methylthiomethyl-4-(S)-methyl-1,3-oxazoline (L), was prepared by the method of Allen et al. [4]. The halogenopentacarbonylrhenium(I) [15] and halogenotrimethylplatinum(IV) [16,17] compounds were synthesised by literature methods. The six complexes were all prepared similarly, as illustrated by the procedure for $[ReBr(CO)_3L]$.

2.1.1. [2-methylthiomethyl-4-(S)-methyl-1,3-oxazoline]bromotricarbonylrhenium(I)

Bromopentacarbonylrhenium(I) (100 mg, 0.25 mmol) and 2-methylthiomethyl-4-(S)-methyl-1,3-oxazoline (50 mg, 0.34 mmol) were refluxed for ca. 18 h in 20 cm^3 of a 50:50 (v/v) mixture of benzene and petroleum ether (boiling pt. 60–80°C). The volatile components were then removed in vacuo, to yield an oily residue. The crude product was purified by crystallisation from a mixture of dichloromethane and pentane. Yield: 108 mg (88%).

2.2. Physical methods

Fast-atom bombardment (FAB) mass spectra were carried out at the London School of Pharmacy on a VG Analytical ZAB-SE instrument, using Xe^+ ion bombardment at 8 kV energy, in a matrix of 3-nitrobenzyl alcohol. Infrared spectra were obtained as CH_2Cl_2 solutions using matched CaF_2 solution cells on a Nicolet 205 FT-IR spectrometer, operating in the region 4000–400 cm^{-1}. Elemental analyses were carried out at University College London.

Hydrogen-1 and ^{13}C NMR spectra were recorded as $CDCl_3$ or $(CDCl_2)_2$ solutions on either a Bruker AMX400 or AMX600 Fourier transform spectrometer, operating at 400.13 or 600.13 MHz for ^1H, and 100.61 or 150.92 MHz for ^{13}C, respectively. Chemical shifts are quoted relative to tetramethylsilane as an internal standard. Platinum-195 spectra were recorded as $CDCl_3$ or $(CDCl_2)_2$ solutions on a Bruker AMX400 Fourier transform spectrometer operating at 86.02 MHz; chemical shifts are quoted relative to the absolute frequency scale, $\Xi(^{195}Pt) = 21.4$ MHz. NMR probe temperatures were controlled by a standard B-VT 2000 unit, and were periodically checked; probe temperatures are considered accurate to within ± 1°C. The line shapes of the variable temperature ^1H NMR spectra were analysed using the iterative simulation program DNMR5 [18]. The 'best-fit' rate constants obtained from the band shape fittings were used to calculate the Eyring activation parameters; the errors quoted are those defined by Binsch and Kessler [19]. Two-dimensional spectra were recorded using standard Bruker automation programs unless otherwise stated (vide infra).

Nuclear Overhauser effect (NOESY) spectra were recorded using NOESYTP [20] which generates the pulse sequence D_1–90°–D_0–90°–D_8–90°-free induction decay. The evolution time, D_0, had an initial value of 3×10^{-6} s and the relaxation delay, D_1, was 2.0 s. Platinum-195 chemical exchange (EXSY) spectra were recorded using the program NOESYTP, which was modified to enable ^1H decoupling in F1 and F2. The initial delay was set at 3×10^{-6} s, D_1 at 1.0 s and the mixing time, D_8, at 0.02 s; the spectral width in F1 and F2 was 27.78 kHz, and total experiment times were ca. 16 h. One-bond $^1H/^{13}C$ chemical shift correlation spectra were acquired using HXCO [21]. Homonuclear ($^1H/^1H$) correlation spectra were obtained using COSYLR [22]; the delay time for the evolution of long range couplings, D_6, was set at 80 ms.

2.3. X-ray crystal structure determination

A colourless single crystal of approximate size 0.74 × 0.42 × 0.24 mm was obtained as described (vide supra), and mounted on a glass fibre. All geometric and intensity data were taken from this sample by an automatic four-circle Nicolet R3 mV diffractometer, using the $\omega - 2\theta$ technique. Three standard reflections (remeasured every 97 scans) showed no significant loss of intensity during collection.

2.3.1. Crystal data and data collection parameters

$C_9H_{11}BrNO_3ReS$, $M = 495.36$, $a = 7.494(3)$, $b = 13.694(8)$, $c = 13.777(8)$ Å, $U = 1414(1)$ Å^3, $T = 293(2)$ K, orthorhombic, space group = $P2_12_12_1$, Mo-Kα radiation ($\lambda = 0.71073$ Å), $Z = 4$, $D_c = 2.327$ mg m^{-3}, $F(000) = 920$, $\mu = 11.57$ mm^{-1}, data collection range $5° \leq 2\theta \leq 50°$, 1431 unique reflection collected.

2.3.2. Structure solution and refinement

Data were corrected for Lorentz, polarisation and (empirically) absorption effects. The structure was solved by direct methods (SHELXS-86) [23] and developed using alternate least-squares refinement on F^2 and Fourier-difference synthesis (SHELXL-93) [24]. Non-hydrogen atoms were refined anisotropically [except for C(2) which was refined isotropically due to nonconvergence of restrained anisotropic refinement]. Hydrogen atoms were inserted in calculated idealised positions [r(C–H) = 0.96 Å] and assigned a common isotropic thermal parameter ($U = 0.08$ Å^2). The final cycle of least-squares included 150 parameters for the 1425 variables, and did not shift any of the parameters by > 0.01 times its standard deviation. The absolute configuration was confirmed by refinement of the Flack parameter to −0.02(5). The final R and $wR(F^2)$ value were 0.0576 and 0.1491, respectively [$R = 0.0541$ and $R_w = 0.1419$ for refinement on F, on 1347 data with the threshold $I > 2\sigma(I)$]; goodness-of-fit on $F^2 = 1.038$. The final Fourier difference map showed three peaks at ca. 2 e Å^{-3}, close to the rhenium atom.

3. Results and discussion

3.1. The complex [ReBr(CO)$_3$L]

The complex *fac*-[ReBr(CO)$_3$L] (L = 2-methylthiomethyl-4-(S)-methyl-1,3-oxazoline) was isolated as a white, air-stable crystalline solid as described (vide supra)

The infrared spectrum displayed three carbonyl stretching bands in the region 1850–2100 cm^{-1}, characteristic of a *fac*-octahedral coordination geometry for the bromotricarbonylrhenium(I) metal moiety [25]. The FAB mass spectrum displayed strong peaks due to $[M]^+$, and $[M\text{-}Br]^+$. Microanalytical data were consistent with the formation of an analytically pure sample of the formulated compound, viz. [ReBr(CO)$_3$($C_6H_{11}NOS$)]. Analytical data are reported in Table 1.

3.1.1. X-ray crystal structure

The X-ray crystal structure of [ReBr(CO)$_3$L] was determined primarily to identify which of the four possible diastereoisomers (Fig. 1) was present, and to confirm the absolute configuration of the ligand. A view of the molecule is shown in Fig. 2, and selected bond lengths and angles are given in Table 2. Fig. 2 clearly shows that the complex crystallises as a single species [**(Ia)** Fig. 1] (there is no disorder), with the oxazole–methyl oriented above the equatorial plane, away from the halide. This might be expected on steric grounds. However, the crystal structure of the related complex [ReCl(CO)$_3${2,6-bis(4-(S)-methyloxazolin-2-yl)pyridine}] [12] reveals that the oxazole–methyl group is oriented on the *same side* as the chloride, implying any steric interactions between the methyl and the halide are minimal. Fig. 2 also shows that the S–Me group is oriented away from the halide, on the same side as the oxazole–methyl. Again, this might be expected on steric grounds; however from previous crystallographic studies on tricarbonylrhenium(I)- and (isoelectronic) trimethylplatinum(IV)-halide complexes of thioether ligands, there appears to be no clear preference for the S–R (R = alkyl or aryl) group to orient either *cis* or *trans* to the halide. The C(10) ··· C(15)[C(S–Me) ··· C(oxazole–Me)] nonbond distance is 5.21 Å.

The metal moiety deviates somewhat from an idealised octahedral coordination geometry. This is due primarily to the 'bite-angle' of the ligand being less than 90°; N(1)–Re–S(1) = 78.1(4)°. The oxazole ring is planar, and is twisted slightly out of the equatorial plane

Table 1
Analytical data for the complexes [ReX(CO)$_3$L] and [PtXMe$_3$L] (X = Cl, Br or I)

Complex	Yield[a] (%)	ν(CO)[b] (cm^{-1})	m/z[c]		Analyses[d] (%)		
					C	H	N
[ReCl(CO)$_3$L]	80	2031.4 1930.3 1899.3	451 416		24.02 (23.97)	2.42 (2.46)	2.97 (3.11)
[ReBr(CO)$_3$L]	88	2032.2 1932.5 1901.4	495 467 416		21.91 (21.82)	2.20 (2.24)	2.68 (2.83)
[ReI(CO)$_3$L]	80	2030.9 1935.3 1903.8	543 416		20.17 (19.93)	1.83 (2.04)	2.28 (2.58)
[PtClMe$_3$L]	43		385 369 355	339 240	25.46 (25.69)	4.81 (4.57)	3.34 (3.33)
[PtBrMe$_3$L]	65		385 369 355	339 240	23.35 (23.23)	4.29 (4.33)	2.86 (3.01)
[PtIMe$_3$L]	60		645 385 369	355 339 240	(21.10)[e]	(3.94)[e]	(2.73)[e]

[a] Yields quoted relative to [ReX(CO)$_5$] or [PtXMe$_3$]$_4$.
[b] Recorded as CH_2Cl_2 solutions.
[c] FAB mass spectral data.
[d] Calculated values in parentheses.
[e] Unreliable analysis (see Section 3.3).

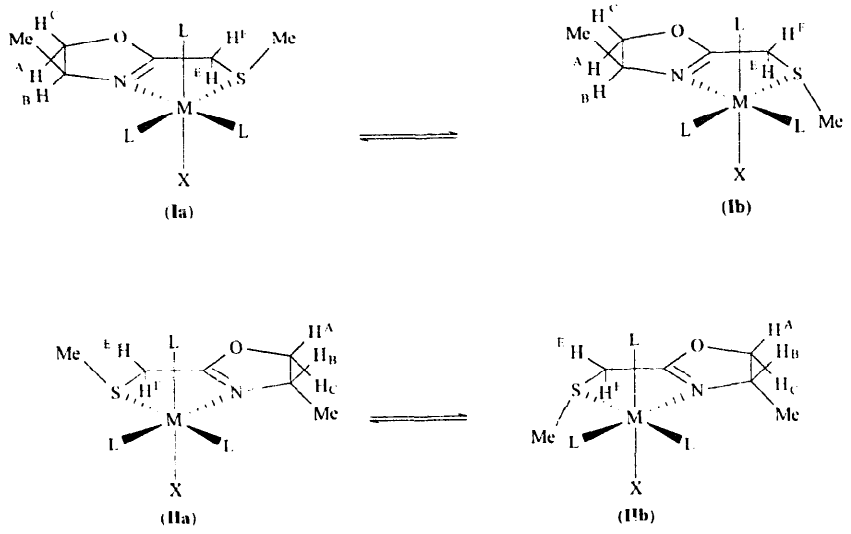

Fig. 1. The four possible diastereoisomers for the complexes $[ReX(CO)_3L]$ and $[PtXMe_3L]$, showing the isomer and hydrogen nuclide labelling schemes, and the two epimerisation pathways.

of the metal moiety (dihedral angle = 15°). The absolute configuration of C(14) (S) is confirmed.

3.1.2. NMR studies

The ambient temperature (298 K) 400 MHz ^{1}H NMR spectrum of the bromo complex, $[ReBr(CO)_3L]$, in $CDCl_3$ displayed two sets of (very) slightly exchange broadened signals, attributable to the two possible diastereoisomers of atropisomer [26] (**I**) (Fig. 1). The diastereisomers arise because of the presence of two possible S invertomers [(**Ia**) and (**Ib**) Fig. 1], which vary according to the orientation of the S–Me group with respect to bromide. The spectra displayed signals in four regions: (i) the oxazole–methyl region (ca. δ = 1.4–1.7); (ii) the S–Me region (ca. δ = 2.6–3.0); (iii) the chelate ring methylene region (ca. δ = 3.4–4.2); (iv) the oxazole–H region (ca. δ = 4.2–5.0). The ^{1}H NMR spectrum at 298 K is shown in Fig. 3, and data are reported in Table 3.

The oxazole–methyl region displayed two doublets [due to coupling of the methyl hydrogen nuclides to H_B (Fig. 1)] of different intensity at δ = 1.56 ($^3J_{HH}$ = 6.5 Hz) and 1.49 ($^3J_{HH}$ = 6.6 Hz), which were assigned to the two possible diastereoisomers, (**Ia**) and (**Ib**). As expected, the S–Me region displayed two singlets, similarly assignable to the two diastereoisomers. The relative populations of the diastereoisomers [77% (major) 23% (minor)] were determined by integration of both the S–Me and oxazole–Me signals.

The oxazole–H and chelate ring methylene regions of the spectrum are more complex. The oxazole ring hydrogen nuclides of each diastereoisomer form the ABC subset of an $ABCD_3$ spin system (the oxazole–Me

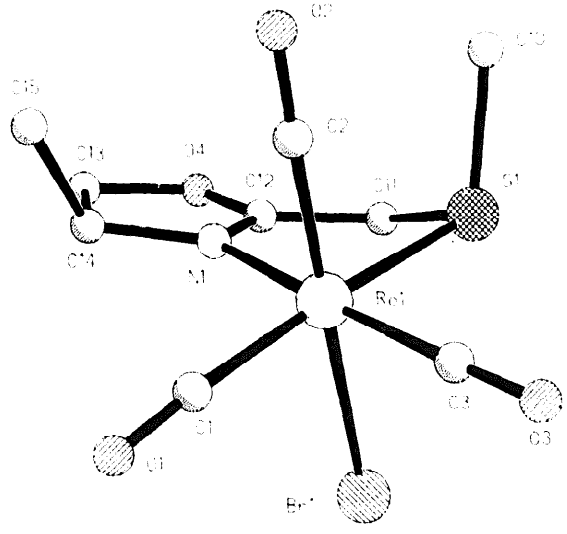

Fig. 2. The X-ray crystal structure of $[ReBr(CO)_3L]$, showing the atomic numbering scheme.

Table 2
Selected bond lengths (Å) and angles (deg) for the complex $[ReBr(CO)_3L]$

Bond lengths (Å)		Bond angles (deg)	
Re(1)–C(1)	1.95(3)	N(1)–Re(1)–S(1)	78.1(4)
Re(1)–C(2)	1.92(2)	C(1)–Re(1)–N(1)	100.6(8)
Re(1)–C(3)	1.94(2)	C(3)–Re(1)–S(1)	95.3(6)
Re(1)–N(1)	2.192(14)	C(1)–Re(1)–C(3)	85.7(9)
Re(1)–S(1)	2.530(5)	C(2)–Re(1)–Br(1)	178.0(6)
Re(1)–Br(1)	2.670(2)	Re(1)–S(1)–C(11)	98.9(6)
S(1)–C(11)	1.82(2)	Re(1)–N(1)–C(12)	122.3(12)
N(1)–C(12)	1.31(2)	N(1)–C(12)–C(11)	123(2)
N(1)–C(14)	1.50(2)	S(1)–C(11)–C(12)	112.5(13)
C(12)–O(4)	1.30(2)	N(1)–C(14)–C(15)	112(2)

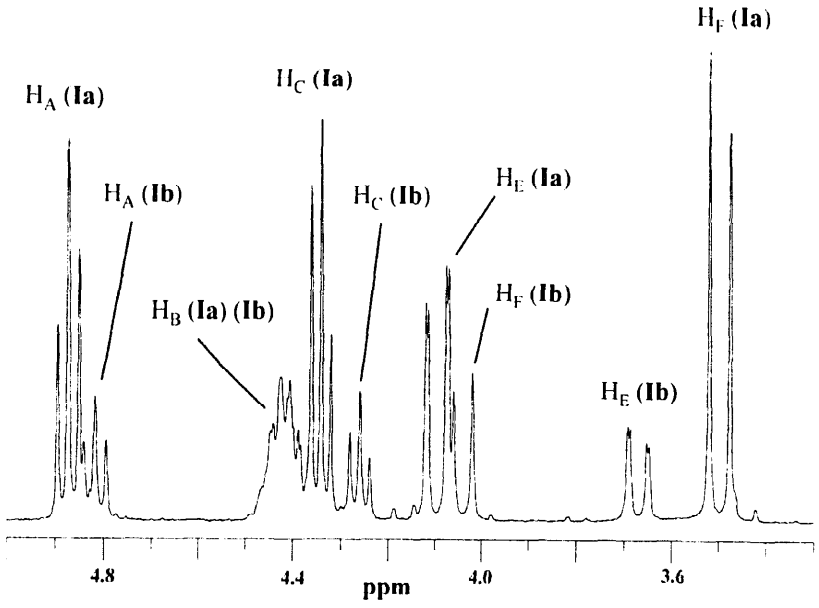

Fig. 3. 400 MHz ^{1}H NMR spectrum of atropisomer (**I**) of [ReBr(CO)$_3$L] in $CDCl_3$ at 298 K, showing the chelate ring–methylene and oxazole–H regions. Refer to Fig. 1 for labelling.

being the D_3 subset); thus each diastereoisomer gives rise to three signals in a 1:1:1 intensity ratio in this region. The sets of signals due to the two diastereoisomers are readily distinguished because of their different intensities. The overlapping signals due to H_B (Fig. 1) are easily assigned because of their complexity; H_B displays $^3J_{HH}$ couplings to the oxazole–methyl (vide supra), and to H_A and H_C. H_B is further complicated by a $^5J_{HH}$ coupling to one of the chelate ring methylene hydrogens (vide infra), giving (in principle) a multiplet of up to 32 lines. H_A and H_C both give rise to triplets as a result of their geminal coupling (to each other) and vicinal coupling to H_B being approximately equal ($\approx$ 8–9 Hz). However, they can be unambiguously distin-

Table 3
Hydrogen-1 NMR data[a] for the complexes [ReX(CO)$_3$L] (X = Cl, Br or I)

Complex	Diastereoisomer[b]	δH_A	δH_C	δH_E	δH_F	δ(oxazole–Me)	δ(S–Me)
[ReCl(CO)$_3$L]	**Ia** (52)	4.81 (9.0[c], 9.0)	4.29 (9.0[c], 9.0)	3.98 (17.5[c], 2.0[d])	3.46 (17.5[c])	1.47 (6.5)	2.65
	Ib (21)	4.75 (9.0[c], 9.0)	4.20 (9.0[c], 9.0)	3.57 (16.3[c], 1.9[d])	4.01 (16.3[c])	1.42 (6.6)	2.73
	IIa (20)	4.80 (8.9[c], 8.9)	4.28 (8.9[c], 8.9)	3.41 (17.1[c], 1.4[d])	4.04 (17.1[c], 1.8[d])	≈ 1.49 (≈ 6.5)	2.67
	IIb (7)	4.71 (8.7[c], 8.7)	4.22 (8.7[c], 8.7)	3.96 (≈ 16[c], 1.7[d])	≈ 3.65[f]	≈ 1.49 (≈ 6.5)	2.74
[ReBr(CO)$_3$L]	**Ia** (77)[e]	4.87 (8.4[c], 8.4)	4.34 (8.4[c], 8.4)	4.10 (17.6[c], 2.0[d])	3.50 (17.6[c])	1.56 (6.5)	2.73
	Ib (23)[e]	4.82 (8.8[c], 8.8)	4.26 (8.8[c], 8.8)	3.67 (16.3[c], 1.8[d])	4.04 (16.3[c])	1.49 (6.6)	2.87
	Ia (54)	4.81 (8.1[c], 8.1)	4.29 (8.1[c], 8.1)	3.98 (17.7[c], 2.1[d])	3.47 (17.7[c])	1.41 (6.6)	2.65
	Ib (17)	4.76 (8.7[c], 8.7)	4.20 (8.7[c], 8.7)	3.58 (16.4[c], 2.2[d])	4.02 (16.4[c])	1.47 (6.4)	2.79
	IIa (22)	4.80 (8.2[c], 8.2)	4.28 (8.2[c], 8.2)	3.42 (17.4[c], 1.5[d])	4.05 (17.4[c], 1.5[d])	≈ 1.49 (≈ 6.3)	2.69
	IIb (7)	4.71 (8.3[c], 8.3)	4.22 (8.3[c], 8.3)	3.97 (15.9[c], 1.3[d])	3.69 (15.9[c], 1.6[d])	≈ 1.49 (≈ 6.3)	2.80
[ReI(CO)$_3$L]	**Ia** (56)	4.80 (7.9[c], 7.9)	4.28 (7.9[c], 7.9)	3.96 (17.9[c], 2.0[d])	3.50 (17.9)	1.50 (6.3)	2.73
	Ib (13)	4.74 (8.9[c], 8.9)	4.18 (8.9[c], 8.9)	3.56 (17.4[c], 2.0[d])	4.02 (17.4[c])	1.40 (6.6)	2.89
	IIa (27)	4.81 (8.3[c], 8.3)	4.27 (8.3[c], 8.3)	3.44 (17.7[c], 1.3[d])	4.05 (17.8[c], 1.8[d])	≈ 1.47 (≈ 5.8)	2.72
	IIb (4)	4.71 (8.4[c], 8.4)	4.21 (8.4[c], 8.4)	≈ 4.0 (15.4[c], [g])	3.72 (15.4[c], 1.7[d])	≈ 1.47 (≈ 5.8)	2.90

[a]Recorded as $(CDCl_2)_2$ solutions at 276 K, except [c] (see Section 3.1.2); chemical shifts quoted in ppm relative to TMS; see Fig. 1 for assignments; $^3J_{HH}$ (Hz) given in parentheses; H_B gives a complex, broad multiplet at ca. 4.3–4.4 ppm for each species.
[b]See Fig. 1 for labelling; % populations given in parentheses.
[c]$^2J_{HH}$ (Hz).
[d]$^5J_{HH}$ (Hz).
[e]Recorded as a $CDCl_3$ solution at 298 K.
[f]Signal overlaps with a band due to a minor impurity.
[g]$^5J_{HH}$ not resolved.

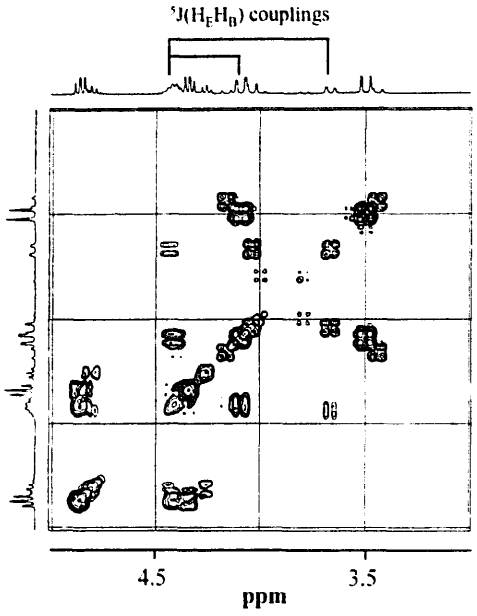

Fig. 4. 400 MHz ^{1}H long range COSY spectrum of atropisomer (**I**) of [ReBr(CO)$_3$L] in $CDCl_3$ at 298 K.

guished by an NOE experiment; H_A and H_B display through space cross-relaxation, but H_B and H_C do not. This assignment is consistent with the relative chemical shifts anticipated for the two environments; H_A would be expected to resonate to higher frequency than H_C [12].

The chelate ring methylene hydrogens of the two diastereoisomers each give rise to a widely spaced AB quartet; again, the signals due to the different diastereoisomers are easily distinguished by their relative intensities. The lower frequency subset of the AB system was assigned to the H atoms *cis* S–Me and the high frequency subset to the H atoms *trans* S–Me on the basis of a NOESY experiment. It is interesting to note that the H environment *trans* the S-methyl in the major isomer, and *cis* the S-methyl in the minor isomer displays a measurable (≈ 2 Hz) ^5J scalar coupling to H_B of the oxazole ring. The character of the coupling was confirmed by a long-range COSY experiment (Fig. 4).

The presence of long range couplings in oxazole rings is well known [27]. However, we are unaware of any studies having been carried out to determine the relative magnitudes of the cisoid and transoid couplings. If it is assumed that the diastereoisomer that is present in the solid-state (Fig. 2) is dominant in solution, then it follows that the magnitude of the cisoid coupling must be greater than the transoid.

The ^{13}C NMR spectrum of [ReBr(CO)$_3$L] (100 MHz; $CDCl_3$; 298 K) also displays two sets of signals due to the two possible diastereoisomers, (**Ia**) and (**Ib**). The assignments of the ligand resonances were made on the basis of DEPT-135 and one-bond ^{1}H/^{13}C heteronuclear chemical shift correlation experiments. Carbon-13 NMR data are reported in Table 4.

On warming a sample of the complex in $(CDCl_2)_2$ above ambient temperature, the ^{1}H NMR lines broadened indicating the onset of pyramidal inversion at the sulfur atom [28] (which gives rise to an exchange of diastereoisomers) at a measurable rate on the NMR chemical shift time scale. Variable temperature spectra were recorded at 5 K intervals from 276 to 382 K, in order to measure the energetics of the epimerisation. However, the band shape changes were not fully reversible, and on cooling two further sets of signals were observed in the 'static' spectrum. These were attributed to the two diastereoisomers of the second possible atropisomer of [ReBr(CO)$_3$L] [(**II**) Fig. 1], which differs from (**I**) in respect of the relationship of the oxazole–methyl to the halide. Thus at elevated temperatures, the complex must undergo some ligand reorientation process, or atropisomerisation. Studies indicate that atropisomerisation takes several hours at ca. 350 K, and several weeks at ca. 273 K. Although structures (**I**) and (**II**) are related effectively by a 180° rotation of the ligand about the N(1)–Re(1)–S(1) bond angle, we tend to the view that the isomerisation probably involves ligand dissociation rather than an intramolecular rotation, hence the terminology 'atropisomers' rather than 'rotomers'.

The ambient temperature 400 MHz ^{1}H NMR spectrum of the solution containing the two atropisomers was difficult to interpret because of significant overlap

Table 4
Carbon-13 NMR data[a] for the complexes [ReX(CO)$_3$L] (X = Cl, Br or I)

Complex	Diastereoisomer[b]	C(10)	C(11)	C(13)	C(14)	C(15)
[ReCl(CO)$_3$L]		25.83	35.42	78.81	64.60	21.63
		25.77	35.53	78.65	64.41	21.44
		19.29[e]	34.82	78.09	63.34	[d]
		[d]	[d]	[d]	[d]	[d]
[ReBr(CO)$_3$L]	(**Ia**)[c]	26.63	36.30	78.72	63.53	21.65
	(**Ib**)[c]	20.67e	35.33	78.17	64.86	21.46
		26.58	36.10	78.67	64.86	21.68
		26.47	35.87	78.52	64.65	21.45
		20.47[e]	35.23	78.11	63.37	21.28
		[d]	34.97	[d]	[d]	20.68
[ReI(CO)$_3$L]		27.74	37.05	78.58	64.93	21.79
		27.54	36.54	78.47	63.42	21.58
		24.00[e]	36.21	78.10	[d]	21.35
		23.20[e]	35.79	[d]	[d]	21.20

[a]Recorded as $(CDCl_2)_2$ solutions at 298 K, except [c] (see Section 3.1.2); chemical shifts quoted in ppm relative to TMS; see Fig. 2 for labelling; the resonance due to C(12) was not observed.
[b]See Fig. 1 for labelling.
[c]Recorded as a $CDCl_3$ solution at 298 K.
[d]Band not observed.
[e]Signal due to the minor S invertomer (diastereoisomer).

of the signals. Spectra were therefore sought at higher field. The 600 MHz ^{1}H NMR spectrum of [ReBr(CO)$_3$L] in $(CDCl_2)_2$ at 276 K is shown in Fig. 5. The spectrum displayed four sets of signals due to the four possible solution-state diastereoisomers shown in Fig. 1, and is essentially analogous to that described for the solution containing only (**Ia**) and (**Ib**) (vide supra). The oxazole–methyl region of the spectrum displays three doublets in a ca. 7:5:2 intensity ratio at $\delta = 1.49$, 1.48 and 1.42, respectively. The two doublets due to (**Ia**) and (**Ib**) were easily identified from their relative intensities. The third doublet ($\delta = 1.49$) was thus presumed to arise from overlap of the two oxazole–methyls due to (**IIa**) and (**IIb**). As expected, the S–Me region displayed four singlets, one for each of the four possible diastereoisomers. The relative populations of the four solution-state species (Table 3) were determined by simulation of the four S–Me signals.

The chelate ring methylene hydrogen nuclides displayed four widely spaced, AB quartets, which were assigned by comparison with the spectrum obtained for atropisomer (**I**). Long-range coupling between H_E and H_B ($^5J_{HH} \approx 1.5$ Hz) is observed in (**II**); however, H_F also appears to be weakly coupled to H_B ($^5J_{HH} \approx 1$–1.5 Hz). Thus the change in conformation of the chelate ring that occurs on atropisomerisation must facilitate a transoid coupling pathway. From the X-ray crystal structure of (**Ia**), the torsional angle between the planes containing C(14)–C(11)–H_B and C(14)–C(11)–H_E (cisoid) is 30°, whereas the torsional angle between C(14)–C(11)–H_B and C(14)–C(11)–H_F (transoid) is 150°. Thus the magnitude of the ^5J coupling of the transoid nuclides (vide infra) appears to be heavily dependent on the torsional angle between them. The conformational change in the chelate ring caused by atropisomerisation presumably leads to the torsional angle between C(14)–C(11)–H_B and C(14)–C(11)–H_F being substantially reduced, hence enabling a measurable ^5J coupling between transoid nuclides to be observed. Since a (slightly reduced) measurable cisoid coupling remains in (**IIa**) and (**IIb**), the cisoid coupling pathway must be less dependent on the torsional angle [which is presumably larger in (**II**) than (**I**)]. This observation may provide a method for probing the solution-state structures of oxazoline complexes in favourable cases.

The oxazole–H region displays four sets of (three) signals. Despite the complexity of the spectrum in this region, a full assignment is possible. The groups of signals due to H_A, H_B and H_C were readily identified by their chemical shifts (Table 3), and within each group, the signals due to the individual diastereoisomers were assigned on the basis of their relative intensities. The 'absolute' assignment of the diastereoisomers in (**II**) is problematic. In (**Ia**) and (**Ib**), H_E and H_F can be distinguished [H_E displays a ^5J coupling to H_B, but H_F does not]. Hence the two diastereoisomers can be differentiated by a NOE experiment; in (**Ia**) a nuclear Overhauser enhancement is observed between the S–Me group and H_F, and in (**Ib**) a NOE is observed between the S–Me group and H_E (vide supra). Since in (**II**), H_E and H_F can not be distinguished (they both display measurable coupling to H_B), it is not possible to differentiate between (**IIa**) and (**IIb**) on the basis of a NOESY experiment. However, we tend to the view that, in keeping atropisomer (**I**), the dominant diastereoisomer

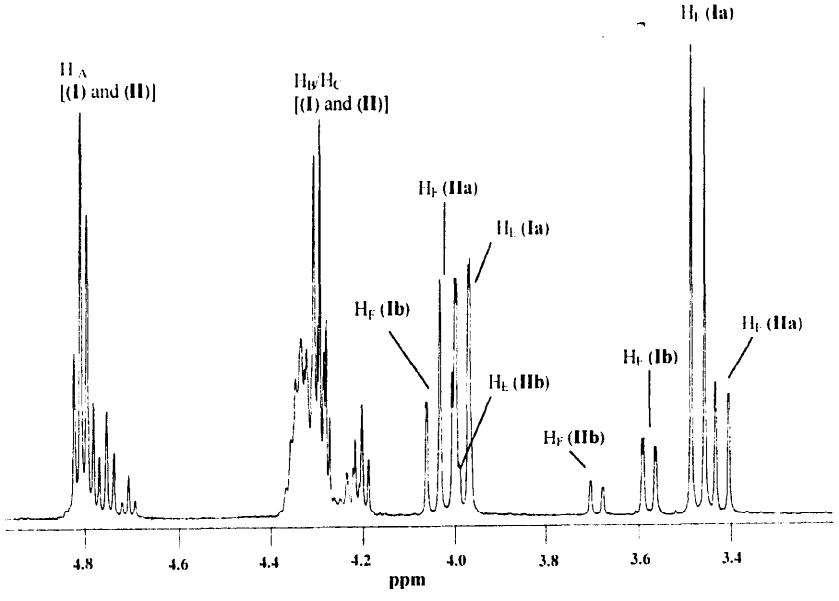

Fig. 5. 600 MHz ^{1}H NMR spectrum of atropisomers (**I**) and (**II**) of [ReBr(CO)$_3$L] in $(CDCl_2)_2$ at 276 K. See Fig. 1 for labelling.

will be the species with the S–Me group oriented away from the halide [i.e. (**IIa**) Fig. 1]. Spectra were assigned on this basis. Hydrogen-1 NMR data are reported in Table 3.

The 150 MHz ^{13}C NMR spectrum in $(CDCl_2)_2$ shows resonances due to each of the four solution-state species; however not all the expected bands were observed. Although it was not possible to unambiguously assign the signals to the different diastereoisomers, an assignment of groups of signals was made on the basis of DEPT-135 and one-bond $^1H/^{13}C$ chemical shift correlation experiments, and data are reported in Table 4. The large chemical shift differences between the S–C(Me) signals are noteworthy. The signals due to the minor diastereoisomers of each atropisomer resonate at much lower frequency than those due to the major diastereoisomers, indicating the high sensitivity of C(10) (Fig. 2) to the orientation of the S–Me group.

Variable temperature ^1H studies were carried out in order to measure the energetics of the epimerisation (i.e., pyramidal inversion at sulfur) in (**I**) and (**II**). Twenty spectra were recorded between 276 and 382 K, and the line shapes of the S–Me signals analysed by standard band shape simulation procedures. The equilibrium between the two atropisomers, (**I**) and (**II**), is slightly temperature dependent (this must be taken into account in the simulation of the temperature dependent spectra), although the rate of atropisomerisation remains negligible on the NMR time scale at all temperatures. Thus in the fast exchange limit, two S–Me signals of different intensity are observed due to the time-averaged spectra of the diastereoisomers of (**I**) and (**II**). Above ca. 340 K, the spectra could not be fitted to unique magnitudes for the two independent rate constants; however, thirteen reliable fits were obtained, five of which are shown in Fig. 6. The Eyring activation parameters are reported in Table 5.

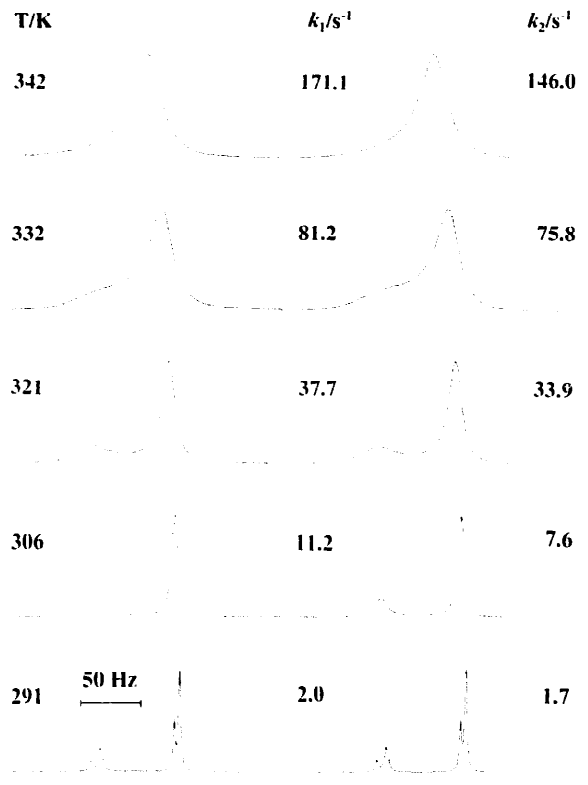

Fig. 6. Variable temperature ^1H NMR spectra of $[ReBr(CO)_3L]$. Computer simulated spectra are shown along side, with the 'best-fit' rate constants. The rate constants k_1 and k_2 refer to the epimerisation processes (**Ia**) → (**Ib**) and (**IIa**) → (**IIb**), respectively.

3.2. The complexes $[ReX(CO)_3L]$

The complexes $[ReX(CO)_3L]$ (X = Cl, or I; L = 2-methylthiomethyl-4-(S)-methyl-1,3-oxazoline) were prepared as white, air-stable crystalline solids as described above. The infrared spectra both displayed three bands in the carbonyl stretching region, characteristic of the metal moiety possessing a fac-octahedral coordination geometry [25]. The mass spectral data and micro analyses were consistent with the presence of the formulated species, viz. $[ReX(CO)_3((C_6H_{11}NOS)]$ (X = Cl or I).

The ambient temperature (298 K) 400 MHz ^1H NMR spectra of the complexes $[ReX(CO)_3L]$ (X = Cl or I) in $CDCl_3$ displayed signals due to all four possible diastereoisomers. Thus unlike $[ReBr(CO)_3L]$, the chloro- and iodo-complexes do not appear to crystallise as a single species, but rather as a mixture of atropisomers. The complexity of the spectra obtained frustrated any

Table 5
Eyring activation parameters[a] for the complexes $[ReX(CO)_3L]$ (X = Cl, Br or I)

Complex	Atropisomer[b]	$\Delta H^{\ddagger}$ (kJ mol^{-1})	$\Delta S^{\ddagger}$ (J mol^{-1} K^{-1})	$\Delta G^{\ddagger}$ (kJ mol^{-1})
$[ReCl(CO)_3L]$	(**I**)	67.5 (0.9)	−0.8 (2.9)	67.77 (0.07)
	(**II**)	67.8 (1.3)	−0.8 (4.1)	68.03 (0.11)
$[ReBr(CO)_3L]$	(**I**)	69.7 (1.3)	1.4 (4.1)	69.32 (0.05)
	(**II**)	71.7 (0.9)	5.9 (3.0)	69.93 (0.03)
$[ReI(CO)_3L]$	(**I**)	70.4 (1.6)	3.0 (5.2)	69.51 (0.07)
	(**II**)	76.4 (2.4)	21.6 (7.6)	69.97 (0.16)

[a]Errors quoted in parentheses; $\Delta G^{\ddagger}$ quoted at 298 K; data refers to the process major diastereoisomer → minor diastereoisomer.
[b]See Fig. 1 for labelling.

detailed analysis, so data were sought at higher field. The 600 MHz ^{1}H and the 150 MHz ^{13}C NMR spectra of the complexes $[ReX(CO)_3L]$ (X = Cl or Br) were essentially identical to the spectra- obtained for $[ReBr(CO)_3L]$. Spectral assignments (^{1}H and ^{13}C) were made on the same basis as that described for $[ReBr(CO)_3L]$. Hydrogen-1 and ^{13}C NMR data are reported in Tables 3 and 4, respectively.

On warming, the ^{1}H NMR signals underwent (fully reversible) dynamic line broadening, indicative of inversion at the S atom. The energetics of the epimerisation were measured by standard band shape analysis of the S–Me signals. Eyring activation parameters are reported in Table 5.

3.2.1. Activation parameters

Examination of the activation parameters obtained for the epimerisation (S inversion) in the complexes $[ReX(CO)_3L]$ (Table 5) reveal several points of interest.

(i) The magnitudes of the free energies of activation [$\Delta G^{\ddagger}$ (298 K)] are in the range 67.7 to 70 kJ mol^{-1}. This is relatively high for pyramidal inversion at S, but is within the range anticipated for rhenium-sufide complexes [28].

(ii) $\Delta G^{\ddagger}$ (298 K) has a small, but consistent halogen dependence in both atropisomers; $\Delta G^{\ddagger}$ Cl < Br < I.

(iii) $\Delta G^{\ddagger}$ (298 K) is slightly greater in atropisomer (II) than atropisomer (I). Since the ground state energies of the diasteroisomers of (II) are higher than (I) (this is evident from the solution-state populations), this presumably results from a small destabilisation of the transition state.

(iv) The entropies of activation, $\Delta S^{\ddagger}$, are close to zero, as expected for an intramolecular pathway.

3.3. The complexes $[PtXMe_3L]$

The complexes $[PtXMe_3L]$ (X = Cl, Br or I; L = 2-methylthiomethyl-4-(S)-methyl-1,3-oxazoline) were prepared as described above, and isolated as colourless, air-stable oils. Solid samples were obtained for X = Cl and Br by washing the oils with a 1:5 (v/v) mixture of acetone:petroleum ether (boiling pt. 60–80°C). The fast atom bombardment mass spectra of all three complexes displayed strong fragmentation peaks due to the species $[M-X]^+$, $[M-X-Me]^+$, $[M-X-2Me]^+$, $[M-X-3Me]^+$ and $[PtMe_3]^+$. The complex $[PtIMe_3L]$ displayed an additional peak at $m/z^+ = 645$ due to $[M + Cs]^+$ (Cs is used to calibrate the spectrometer). Microanalytical data were generally consistent with the proposed formulation; however, it was not possible to obtain an analytically pure sample of $[PtIMe_3L]$ (vide supra). Analytical data are reported in Table 1.

3.3.1. NMR studies

The ambient temperature (298 K) 600 MHz ^{1}H NMR spectra of the complexes $[PtXMe_3L]$ (X = Cl, Br or I; L = 2-methylthiomethyl-4-(S)-methyl-1,3-oxazoline) were highly complex owing to the presence of four overlapping sets of signals due to the four possible solution-state diasteroisomers (Fig. 1). The spectra were analogous to those obtained for the rhenium(I) complexes, except for the presence of twelve additional signals (with ^{195}Pt satellites), due to the three different Pt–Me environments in each of the four species. The presence of the Pt–Me bands, which overlapped with the oxazole–Me resonances, and the small chemical shift differences between signals, frustrated attempts to

Table 6
Platinum-195 NMR data[a] for the complexes $[PtXMe_3L]$ (X = Cl, Br or I)

Complex	Solvent	Temperature (K)	$\delta(^{195}Pt)$
$[PtClMe_3L]$	$CDCl_3$	245	1834.5(a)
			1832.6(b)
			1819.0(a)
			1815.0(b)
$[PtBrMe_3L]$	$(CDCl2)_2$	298	
			1762.1(a)
			1753.5(b)
			1723.0(a)
			1716.2(b)
$[PtIMe_3L]$	$(CDCl2)_2$	298	1593.2(a)
			1570.4(b)
			1515.9(a)
			1498.0(b)

[a]Chemical shifts quoted in ppm relative to the absolute frequency scale, $\Xi(^{195}Pt) = 21.4$ MHz; pairs of diastereoisomers are labelled (a) and (b).

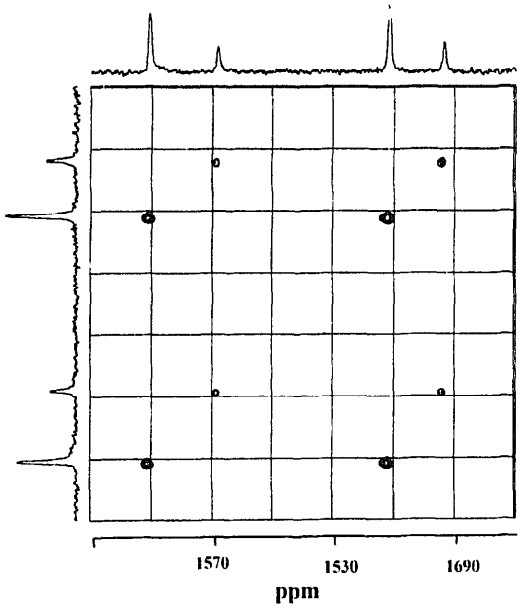

Fig. 7. Platinum-195 2D EXSY spectrum of $[PtIMe_3L]$ at 298 K. Cross peaks are clearly visible between pairs of diastereoisomers, as a result of pyramidal inversion at the S atom.

analyse the spectra. Platinum-195 NMR spectra were therefore acquired.

The ambient temperature ^{195}Pt NMR spectra of the complexes [$PtXMe_3L$] (X = Br or I) displayed four peaks; one due to each of the four possible solution-state diastereoisomers. In the case of the chloro complex, [$PtClMe_3L$], only two bands were observed; however on cooling, two additional (broad) signals appeared above the baseline. On further cooling, these sharpened, and at ca. 240 K, four non-exchange broadened bands were observed. Platinum-195 NMR data are reported in Table 6.

On warming, these bands exhibited reversible dynamic line broadening, indicative of pyramidal inversion at the S atom. However, the large chemical shift differences between pairs of diastereoisomers prevented any dynamic data from being measured by conventional band shape analysis methods (the highly exchange broadened signals were not visible above the base line). Platnium-195 two-dimensional EXSY spectra were therefore acquired. The ^{195}Pt 2D EXSY spectrum of [$PtIMe_3L$] at 298 K is shown in Fig. 7. This clearly shows cross peaks between pairs of signals, and enables the bands due to the two sets of diastereoisomers to be identified. However, it is not possible assign unambiguously individual signals to a particular diastereoisomer (or even pairs of signals to a particular atropisomer). A quantitative study of the S inversion was not undertaken because of the prolonged acquisition times necessary for ^{195}Pt EXSY spectra (S inversion is a well-established process [28] and it was felt unlikely that any significant new information would be obtained).

4. Conclusion

Detailed analysis of the NMR spectra of the complexes [$ReX(CO)_3L$] and [$PtXMe_3L$] (X = Cl, Br or I; L = 2-methylthiomethyl-4-(S)-methyl-1,3-oxazoline) reveals that they form two chemically distinct atropisomers, which differ in respect of the orientation of the oxazole–Me group to the halide. In solution, each atropisomer gives rise to a pair of diastereoisomers, which result from the two possible S invertomers. At moderate temperatures, pyramidal inversion at the coordinated S atom leads to the epimerisation of pairs of diastereoisomers; however atropisomerisation remains slow on the NMR time szcale even at temperatures above 100°C.

Acknowledgements

We are grateful to the University of London for access to the ULIRS NMR services at Kings College, and Queen Mary and Westfield College.

References

[1] A.I. Meyers, P.M. Kendall, Tetrahedron Lett. 15 (1974) 1337.
[2] A.I. Meyers, M.E. Ford, Tetrahedron Lett. 15 (1974) 1341.
[3] T.G. Gant, A.I. Meyers, Tetrahedron 50 (1994) 2297, and refs. therein.
[4] J.V. Allen, G.J. Dawson, C.G. Frost, J.M.J. Williams, S.J. Coote, Tetrahedron 50 (1994) 799.
[5] J. Sptinz, G. Helmchen, Tetrahedron Lett. 34 (1993) 1769.
[6] C.G. Frost, J.M.J. Williams, Tetrahedron Lett. 34 (1993) 2015.
[7] G.J. Dawson, C.G. Frost, J.M.J. Williams, S.J. Coote, Tetrahedron Lett. 34 (1993) 3149.
[8] C.G. Frost, J.M.J. Williams, Synlett. (1994) 551.
[9] Q.-L. Zhou, A. Pfaltz, Tetrahedron 50 (1994) 4467.
[10] G.C. Lloyd-Jones, A. Pfaltz, Angew. Chem., Int. Ed. Engl. 34 (1995) 462.
[11] O. Loiseleur, P. Meier, A. Pfaltz, Angew. Chem., Int. Ed. Engl. 35 (1996) 200.
[12] P.J. Heard, C. Jones, J. Chem. Soc., Dalton Trans. (1997) 1083.
[13] D.F. Shriver, Manipulation of Air-Sensitive Compounds, McGraw-Hill, New York, 1969.
[14] D.D. Perrin, W.L.F. Armarego, Purification of Laboratory Chemicals, Pergamon, Oxford, 1988.
[15] S.P. Schmidt, W.C. Trogler, F. Basolo, Inorg. Synth. 28 (1979) 160.
[16] J.C. Baldwin, W.C. Kaska, Inorg. Chem. 14 (1975) 2020.
[17] D.H. Goldsworthy, PhD thesis, University of Exeter, 1980.
[18] D.S. Stephenson, G. Binsch, DNMR5, Quantum Chemistry Program Exchange, Indiana University.
[19] G. Binsch, H. Kessler, Angew. Chem., Int. Ed. Engl. 19 (1980) 411.
[20] G. Bodenhausen, H. Kogler, R.R. Ernst, J. Magn. Reson. 58 (1984) 34.
[21] A. Bax, G.A. Morris, J. Magn. Reson. 42 (1981) 501.
[22] A. Bax, R. Freeman, J. Magn. Reson. 44 (1981) 542.
[23] G.M. Sheldrick, Acta Crystallogr. 46 (1990) 467, Sect. A.
[24] G.M. Sheldrick, SHELEXL-93, University of Göttingen, 1993.
[25] D.A. Edwards, J. Marshalsea, J. Organomet. Chem. 131 (1977) 73.
[26] E.L. Eliel, S.H. Wilen, Stereochemistry of Organic Compounds, Wiley, New York, 1994.
[27] S. Sternhell, Rev. Pure Appl. Chem. 14 (1964) 15.
[28] E.W. Abel, S.K. Bhargava, K.G. Orrell, Prog. Inorg. Chem. 32 (1984) 1.